Mean surface runoff insensitive to warming in a key Mediterranean-type climate: A case study of the Los Angeles Region

Marla Schwartz[1]
University of California, Los Angeles

Alex Hall
University of California, Los Angeles

Fengpeng Sun
University of California, Los Angeles

[1] *Corresponding author address: Marla Schwartz, Math Science Bldg Rm 7229, UCLA, Department of Atmospheric and Oceanic Sciences, Los Angeles CA 90095.*
Email: marla@atmos.ucla.edu

Abstract

This paper investigates the sensitivity of surface hydrology in the Los Angeles region to climate change. Using dynamical downscaling, we produce 2-km resolution regional projections for the mid-21st century (2041-2060) under the "business-as-usual" (RCP8.5) forcing scenario for five global climate models in the Fifth Coupled Model Intercomparison Project. Future projections are compared to a validated reanalysis-driven simulation of a baseline period (1981-2000) to quantify surface hydrology changes. Precipitation changes are likely to be small and are within the range of baseline interannual variability. Runoff changes are strongly controlled by precipitation changes, suggesting temperature-driven changes in actual evapotranspiration are small. A series of temperature sensitivity experiments are performed in which a land surface model is forced by the meteorology of the baseline period, but with uniform near-surface air temperature increases of 2º, 4º and 6º C. Results from these idealized experiments reveal annual mean actual evapotranspiration and runoff are nearly insensitive to warming. This insensitivity is an artifact of the region's Mediterranean-type climate: Because the warm season receives almost no precipitation, the strongest warming-induced potential evapotranspiration enhancement coincides with dry soils, severely constraining actual evapotranspiration increases. Surface hydrology in other Mediterranean climate regions may respond similarly. This result greatly mitigates a potential vulnerability of water resources to a changing climate in an important semi-arid region of the world. It also reveals that a regional climate change adaptation strategy relying on local water resources is a viable one.

1. Introduction

Mediterranean-type climate zones (California, lands around the Mediterranean Sea, central Chile, southwestern South Africa, and southwestern and southern Australia) are characterized by warm, dry summers and cool, rainy winters (Myers et al. 2000; Cowling et al. 2005; Kottek et al. 2006). The florae of these regions are among the world's richest, harboring almost 20% of all known vascular plant species despite occupying less than 5% of the earth's surface (Cowling et al. 1996). Mediterranean-type climate regions have also been recognized as particularly threatened by global climate change (IPCC 2014).

A potentially unique surface hydrological response to climate change may arise from the seasonality of Mediterranean-type hydrology. Projected temperature increases, along with increased downward longwave radiation from greater concentrations of greenhouse gases, would enhance potential evapotranspiration (PET). The enhancement is especially large in the warm months, due to the non-linearity of the Clausius-Clayeron relationship. However, because rain comes during the cool months, soil moisture levels are low during the warm months. As a result, the time of the strongest PET enhancement may coincide with the driest soils. Thus it is unclear whether actual evapotranspiration (AET) will respond strongly to warming. Surface runoff may likewise be only weakly affected by warming. Therefore, it is important to investigate how climate-change induced temperature and precipitation changes will impact surface hydrology in Mediterranean-type climate regions.

This paper explores the hydrologic response of California's Los Angeles region as a case study. Previous studies have documented observed changes in California's hydro-climate over the past few decades, as well as potential impacts in hydrology and water resources in the western United States (Roos 1991; Hamlet et al. 2005; Maurer 2007; Barnett et al. 2008; Bates et al. 2008; Adam et al. 2009; Kapnick and Hall 2010). However, a high-resolution assessment of the response of surface hydrology in the Los Angeles region to climate change has not been done before.

This study is informative due to its implications for other Mediterranean-type climate zones, and it is crucial for informed local water resources planning. The Greater Los Angeles region depends on numerous sources of fresh water, both imported and local. Though the majority of Los Angeles' water is imported via the Los Angeles and Colorado River Aqueducts, local water accounted for 11% of the Los Angeles Department of Water and Power's water supply from 2005-2010 (Blanco et al. 2012). In some nearby cities within the Greater Los Angeles region, local water sources contribute an even larger portion. For example, local water supplied about 40% of the overall water demand between 1995 and 2009 in the city of Camarillo (City of Camarillo 2010) and 55% of the water demand in Long Beach for 2010 (Long Beach Water Department 2010).

Cities in Mediterranean-type climates outside of California also rely heavily on local water, including Cape Town, South Africa, which chiefly depends on dams in the mountains of the southwestern Cape for both industrial and domestic water supply (Ziervogel et al. 2010). Adelaide, Australia sources water from neighboring catchments in the Mount Lofty Ranges and approximately half of Adelaide's demand has been supplied from the nearby Myponga, Mount

Bold, and Happy Valley reservoirs (Paton et al. 2013). In central Chile, snowpack accumulated in the nearby central Andes represents a critical resource for local irrigation, consumption, industries and hydroelectric generation (Masiokas et al. 2006).

General circulation models (GCMs) provide insight into future climate trends, but their coarse resolution fails to capture climatic variables at a scale necessary for regional-scale analysis (Giorgi and Mearns, 1991). The latest generation of GCMs in the World Climate Research Programme's Coupled Model Intercomparison Project Phase 5 (CMIP5; Taylor et al. 2012) have horizontal resolutions between 1° to 2.5° (~ 100 – 250 km). Los Angeles' complex coastlines and topographical features show variation on much smaller scales and play a dominant role in shaping regional-scale processes, including orographic precipitation, land-sea breezes and valley circulations. Additionally, local topography introduces large spatial gradients in surface and near-surface air temperature, which influence PET. Such regional-scale processes have been shown to be critical in understanding climate variability in California (Cayan, 1996; Conil and Hall, 2006; Hughes et al. 2007). Thus, current GCM resolution is far too low to understand surface hydrology and climate at scales relevant for adaptation and water resources planning.

Dynamical-downscaling has been used to develop high-resolution regional climate data from relatively coarse-resolution GCM output, including in California (Leung et al. 2003; Leung et al. 2004; Kanamitsu and Kanamaru 2007; Caldwell et al. 2009; Qian et al. 2010; Pan et al. 2011; Pierce et al. 2012) and other Mediterranean-type climate regions (Flaounas et al. 2012; Barrera-Escoda et al. 2013; Ratnam et al. 2013). The dynamical downscaling studies over California, along with a number of regional studies using hydrological models (Dettinger et al. 2004;

Vicuna et al. 2007; Young et al. 2009; Huang et al. 2012), have focused primarily on climate change impacts to hydrology in Central and Northern California, rather than the Los Angeles region.

In this study, dynamical-downscaling simulations are performed to obtain high-resolution (2-km) climate information for the Los Angeles region. These consist of a validated baseline (1981-2000) climate simulation, and downscaling of output from five CMIP5 GCMs under Representative Concentration Pathway 8.5 (RCP8.5) for the mid-21st century period (2041-2060). Idealized temperature sensitivity experiments are also performed, in which the baseline climate simulation is perturbed by uniform air temperature increases of 2º, 4º and 6º C. These experiments reveal the hydrologic sensitivity to warming in the absence of precipitation change. This is a relevant simplification because the projected annual precipitation changes turn out to be quite small in this region (Berg et al. 2015). This study aims to assess changes to runoff and AET that result from precipitation and temperature changes in both the Los Angeles region and other Mediterranean-type climate regions. In the process, we will determine the degree to which sensitivity of AET and runoff to warming is indeed suppressed by the unique seasonality of Mediterranean-type climate.

This study is part of a larger project that includes separate downscaling studies of the CMIP5 ensemble's mid-21st century and end-of-21st century projections over the Los Angeles region for temperature (Walton et al. 2015; Sun et al. 2015a), precipitation (Berg et al. 2015), and snowfall and snowpack (Sun et al. 2015b). Together, these studies provide high-resolution information regarding future regional climate trends crucial for developing effective adaptation strategies.

This paper is organized as follows: Section 2 describes the model configuration and observational evaluation for the baseline simulation. Section 3 describes the future and idealized climate simulations. Section 4 presents the results of both the dynamical-downscaling simulations and the idealized temperature sensitivity experiments. This section is focused on the sensitivity of annual mean AET and runoff to both precipitation and temperature changes, while also placing changes within the context of internal interannual variability. Finally, section 5 presents a discussion of the results, as well as a summary of findings.

2. Baseline Simulation

a) Dynamical downscaling framework

A dynamical downscaling simulation over the Los Angeles region is performed using the Weather Research and Forecasting Model version 3.2 (WRF; Skamarock et al. 2008). We nest higher resolution domains within one another (18-km, 6-km and 2-km) to reach a high enough resolution to represent the most important features of the region's complex topography and coastlines. Fig. 1a shows the three nested domains, as well as the topography at the resolution of the outermost domain. The outermost domain spans the entire state of California and the adjacent Pacific Ocean at 18-km resolution. The middle domain, at 6-km resolution, covers roughly the southern half of the state of California. Finally, the innermost domain, at 2-km resolution, focuses on the Los Angeles region (Fig. 1b). In the downscaling simulations, the Noah Land Surface Model (Chen and Dudhia 2001) is coupled to WRF to simulate land surface processes.

For additional information on parameterization options and WRF configuration settings used in the baseline simulation, the reader is directed to Walton et al. (2015).

Using this model configuration, we perform a twenty-year reanalysis-driven “baseline” simulation, which runs from September 1981 to August 2001. The baseline climate simulation is a dynamical downscaling of the National Centers for Environmental Prediction’s North America Regional Reanalysis (NARR; Mesinger et al. 2006). NARR is a coarse-resolution (32-km) reanalysis dataset that provides the lateral boundary conditions for the outermost nested WRF domain seen in Fig. 1a. This simulation reconstructs weather and climate and serves two purposes. First, it allows us to evaluate the model’s ability to simulate regional climate based on a comparison to observational data. Second, it serves as a climate state against which we can compare future climate simulations to measure climate change.

WRF is reinitialized each year in August, allowing us to run twenty one-year runs from September to August in parallel. This parallelization significantly reduces computational time. However, the annual model re-initialization prevents perfect water budget closure. To ensure the water budget is precisely closed, WRF data from the innermost (2-km) domain of the twenty one-year baseline simulations is used as forcing for a continuous twenty-year simulation using the offline 1-dimensional Noah Land Surface Model version 3.3 (Noah-LSM; Ek et al. 2003). The baseline Noah-LSM simulation is forced by WRF meteorological data, including near-surface air temperature, surface pressure, near-surface wind speed and direction, near-surface relative humidity, precipitation, and downward longwave and shortwave radiative fluxes at the surface. WRF output includes snapshots of 2-dimensional variables every 3 hours and 3-

dimensional variables every 6 hours for each grid point. Output from the offline Noah-LSM simulation forced by WRF output (hereinafter called Noah-LSM/WRF) precisely satisfies the surface water balance equation, solving the water budget closure issue presented by model re-initialization. As the focus of our study is terrestrial surface hydrology, we exclude ocean, lake, reservoir and urban grid points in our analysis.

b) Baseline surface hydro-climate

Fig. 2 shows spatial patterns of climatological precipitation, runoff and AET for the baseline period as simulated by Noah-LSM/WRF. The average annual precipitation received at non-urban land points during the baseline period (Fig. 2a) is 341 mm/yr, with 91% of the study domain's annual precipitation falling between the months of October and April. The coastal side of mountain areas above 1000m receive nearly 3 times the annual precipitation of low-elevation coastal areas due to orographic precipitation effects. The coastal areas experience greater than 200mm more precipitation than the inland desert region, as moisture is wrung out of air passing over the mountain ranges toward the inland desert.

Figs. 2b and 2c present the partitioning of precipitation for the baseline Noah-LSM/WRF simulation into runoff and AET, respectively. In this semi-arid domain, 81% of annual precipitation falling on non-urban land surfaces is returned to the atmosphere through AET, on average. The ratio of runoff to precipitation is highest in coastal areas above 1000m, where runoff accounts for 41% of average incoming annual precipitation.

The annual cycle of the water balance for the baseline period is shown in Fig. 3 for two representative points in our study domain: a high-elevation mountain location (Fig. 3a) and an inland desert location (Fig. 3b). These two locations are shown in Fig. 1b by blue and red circles. The region's climate is characterized by drastic seasonal precipitation variations (especially at the high elevations) and modest seasonal transitions in temperature. In the case of the mountain location, precipitation (blue) peaks in February, and early spring snowmelt leads to maxima in both soil moisture (red) and runoff (cyan) in March. Increasing PET (black) in the late spring and early summer coincides with moist springtime soils (red), so AET (green) increases in the summer months until the soil moisture is depleted. This creates a July peak in AET. The out-of-phase relationship in the annual cycles of precipitation and PET sets up a unique response to temperature changes that will be explored later in this paper. At the desert location, annual precipitation is low, and AET is roughly equal to precipitation, accounting for over 98% of annual mean precipitation.

c) Model evaluation

Prior to analyzing surface hydrology changes, we evaluate the skill of the 2-km resolution baseline (1981-2000) simulation by comparing Noah-LSM/WRF model output to available observations.

We first briefly recapitulate an evaluation of WRF's precipitation by Berg et al. (2015). This downscaling study of precipitation changes over the Los Angeles region uses the same baseline dynamical downscaling framework as this study. Berg et al. (2015) demonstrate that this modeling framework realistically simulates wet-season (December – March) precipitation in the study domain using precipitation gauges from the California Department of Water Resources' California Irrigation Management Information System (CIMIS, http://wwwcimis.water.ca.gov/), and two gridded observational products, NOAA Climate Prediction Center Daily US UNIFIED Precipitation (CPC, http://www.esrl.noaa.gov/psd/data/gridded/data.unified.html) and the University of Delaware Precipitation product (Udel, http://www.esrl.noaa.gov/psd/data/gridded/data.UDel_AirT_Precip.html). They find a high domain-average correlation coefficient (r =0.82) between wet-season (December – March) precipitation observed at CPC grid cells and that simulated at the nearest corresponding WRF grid cell. Overall, they find that WRF simulates monthly precipitation variations at thirteen CIMIS gauges in the study domain reasonably well, and that the WRF framework realistically simulates interannual variability in wet-season precipitation.

Next, we evaluate Noah-LSM/WRF's simulation of streamflow, relying on the United States Geological Survey Hydro-Climatic Data Network-2009 (USGS HCDN-2009, http://waterdata/usgs.gov/nwis/) observational dataset. The USGS HCDN-2009 is a network of streamflow gauges across the United States identified as having: (1) natural streamflow least affected by direct human activities, (2) accurate measurement records, and (3) at least 20 years of complete and continuous discharge record through water year 2009 (Slack et al. 1993; Lins 2012). We obtained daily, quality-controlled streamflow data from 3 stations for which data was available within our study domain for the baseline period. The locations of these streamflow gauges is shown in Fig. 1b by black circles. There is no runoff routing scheme in the Noah-LSM/WRF framework. To account for this, we compare the observed streamflow measurement at a USGS gauge to the sum of simulated surface runoff from all grid points within a watershed upstream of the gauge. This rather primitive form of runoff routing does not account for groundwater dynamics or interactions between groundwater and surface runoff.

Fig. 4a compares monthly climatological average streamflow for USGS gauges with that simulated by Noah-LSM/WRF. Noah-LSM/WRF's simulation of the annual streamflow cycle is consistent with observations for each of the three gauges, with a correlation averaged across the gauges of r = 0.88. In addition, the points fall along the one-to-one line on the plot. Noah-LSM/WRF correctly simulates the magnitude and phasing of heightened streamflows in the months of February through May (late in the wet season), with relatively low flows the rest of the year. The root mean squared error of all data points in Fig. 4a is 0.28 cubic meters per second. These minor differences may be due to observational error or a lack of groundwater dynamics in Noah-LSM/WRF. Fig. 4b compares the annual average streamflow between each USGS gauge and the Noah-LSM/WRF simulation of runoff within the watershed for all twenty water years (September – August) of the baseline period. Correlations above r = 0.69 are found at all gauges, and the gauge-average correlation is r = 0.77. Again, the points fall approximately on the one-to-one line. Overall, Figs. 4a and 4b demonstrate Noah-LSM/WRF reproduces the spatial, seasonal and interannual variations in surface runoff reasonably well.

Unfortunately, observational data networks, including FLUXNET (Balhocchi et al. 2001) and CIMIS stations, do not provide observations of AET (e.g. through measurement methods such as eddy covariance techniques, a scintillometer or lysimeter) in the study domain during the baseline period. This prevents us from comparing simulated AET to observations directly.

However, assuming no mean change in terrestrial water storage on annual time scales, annual mean AET must equal annual mean precipitation minus mean runoff. Because of the skill of Noah-LSM/WRF in realistically simulating interannual variability in both precipitation (Berg et al. 2015) and runoff (Fig. 4b), we can infer the model probably also realistically simulates the interannual variability in AET. Moreover, Noah-LSM/WRF's ability to accurately reproduce seasonal variations in precipitation (Berg et al. 2015) and runoff (Fig. 4a) gives us confidence in the modeling framework's ability to simulate seasonal and spatial variations in AET.

Overall, Fig. 4 and Berg et al. (2015) show that the Noah-LSM/WRF framework simulates the temporal and spatial variations of surface hydrology during the baseline period with reasonable accuracy where reliable observational data are available. Previous research also demonstrates that the WRF framework used in this study provides realistic simulations of both spatial and temporal patterns of temperature (Walton et al. 2015) and snowfall (Sun et al. 2015b). Based on this evidence, it seems likely that the model is able to realistically reproduce the temporal and spatial variations in AET and runoff across the domain, at locations where observations are not available.

3. Future Simulation

Using the same WRF configuration as the baseline climate simulation, we perform a second group of climate simulations designed to simulate a range of future regional climate states corresponding to the mid-21st century. By looking at differences between the future and baseline periods, mid-century changes to surface hydrology relative to the late 20th century can be quantified and evaluated. To produce boundary conditions for future simulations, we employ a previously used method (Schar et al. 1996; Hara et al. 2008; Kawase et al. 2009; Rasmussen et al. 2011), in which future climate is estimated by adding a perturbation reflective of the mean climate change to reanalysis data. We apply this technique to output from five CMIP5 global climate models (CCSM4, CNRM-CM5, GFDL-CM3, MIROC-ESM-CHEM and MPI-ESM-LR) under the RCP8.5 emissions scenario for the mid-21st century period. More specifically, we perturb the NARR baseline boundary conditions (September 1981 - August 2001) by monthly-averaged differences between the future and baseline (2041-2060 minus 1981-2000) climate for each GCM. This perturbation method assumes no change in synoptic and interannual variability at the lateral boundaries. As a result, the frequency of future weather events is very similar to that of the baseline simulation (though we cannot exclude the possibility that regional climate dynamics might alter local weather events). Thus our analysis focuses on time scales of months to years.

Because it would be prohibitively expensive to perform full twenty-year future dynamical-downscaling simulations for each of the five GCMs, we first perform a future twenty-year simulation (September 2041 to August 2061) using climate change signals in CCSM4. Then we examine this experiment to assess whether short simulations can provide statistics robust enough to characterize the regional climate change signal of the full twenty-year simulation. Similar to the baseline simulation, this future simulation is reinitialized every August and run in parallel as twenty one-year simulations. Using Noah-LSM, we also perform a separate continuous twenty-year simulation of the dynamically downscaled output associated with CCSM4.

We find that we are able to capture to a high degree of accuracy the full 20-year runoff and AET signals by simulating only three future years of CCSM4. (We happened to choose September 2058 to August 2061.) For example, averaged over non-urban land points, the 20-year and 3-year runoff signals associated with CCSM4 are -17.6 and -16.3 mm/yr, respectively. Previous analyses of this output found that the 20-year precipitation and temperature signals could also be captured with a high degree of precision by only dynamically-downscaling three future years (Berg et al. 2015; Walton et al. 2015). Thus, to conserve computational resources, we only dynamically downscale the remaining four GCMs (CNRM-CM5, GFDL-CM3, MIROC-ESM-CHEM and MPI-ESM-LR) for three years. For each of these four future simulations, WRF boundary conditions are created by adding the 20-year GCM climate change signal (2041–2060 minus 1981–2000) to NARR data corresponding to September 1998 to August 2001. Though the future simulations of CNRM-CM5, GFDL-CM3, MIROC-ESM-CHEM and MPI-ESM-LR are only three years long, the climate change forcings therefore reflect that of a 20-year averaging period.

Similar to the twenty-year baseline and twenty-year CCSM4 simulations, the three-year mid-21st century simulations associated with CNRM-CM5, GFDL-CM3, MIROC-ESM-CHEM and MPI-ESM-LR are run as three one-year simulations re-initialized every August. The WRF output is then used to force a continuous three-year future climate simulation using Noah-LSM.

Given projections for little to no ensemble-mean precipitation change in our study domain (discussed in section 4a and Berg et al. 2015), it is useful and relevant to study the hydrologic response to warming in isolation from precipitation changes. Thus, we perform three idealized twenty-year simulations with Noah-LSM designed to isolate the imprint of warming on runoff and AET. The idealized simulations are identical to the twenty-year Noah-LSM baseline (1981-2000) simulation forced by WRF data, except with a spatially uniform 2-meter air temperature increase of 2 °C, 4 °C and 6 °C at every time step. All other climatic variables are unchanged from baseline values. The idealized simulations allow us to examine the sensitivity of surface hydrology in the Los Angeles region to a range of likely temperature changes (Walton et al. 2015). Increases in near-surface air temperature can affect runoff characteristics by altering the form of precipitation, AET rate and snowmelt timing. We label the results from the idealized simulations as baseline, T2, T4 and T6.

4. Results

In this section, we present results from both Noah-LSM/WRF dynamical-downscaling of GCM output and the idealized simulations.

a) Small precipitation changes

Fig. 5 (first row) shows annual mean precipitation changes for five GCMs as simulated by Noah-LSM/WRF. The precipitation projections show some intermodel spread, particularly with regard to the sign of the change. The ensemble-mean precipitation change for non-urban land surfaces across the five GCMs is -6.6 mm/yr, a minute change reflective of a cancellation between moistening (CNRM-CM5 and MPI-ESM-LR) and drying (CCSM4, GFDL-CM3 and MIROC-

ESM-CHEM) models. CNRM-CM5 and GFDL-CM3 project the largest precipitation changes, with changes of +51 and –39 mm/yr averaged over non-urban land surfaces, respectively.

These signals in precipitation changes are modest compared to the region's interannual variability. The standard deviation of baseline (1981-2000) precipitation averaged over non-urban land surfaces as simulated by Noah-LSM/WRF is 153 mm/yr, roughly 40% of the climatological mean and reflective of the region's significant interannual hydroclimate variability. Thus the downscaled change in average precipitation over non-urban land surfaces as projected by even the most extreme model (CNRM-CM5) is only about a third of the baseline interannual variability. Berg et al. (2015) further explore the region's precipitation changes, and conclude that the most likely result is a small change in mean precipitation compared to natural variability, with the sign of the change being uncertain. Berg et al. (2015) also extend the analysis to include the full CMIP5 GCM ensemble through statistical techniques. However, their results are very similar to those obtained from dynamically downscaling only these five GCMs.

b) Runoff, AET and PET changes

Annual mean runoff changes for the five GCMs are shown in Fig. 5 (second row). For each GCM, the runoff change mirrors the precipitation change in both sign and magnitude. Fig. 6 corroborates this. The spatial patterns of precipitation change and runoff change are tightly correlated for all models, with a model-average spatial correlation coefficient of $r = 0.88$. For all five future simulations, the sign of the change in annual runoff is the same as the sign of the change in annual precipitation for over 98% of non-urban land grid points in the study domain.

Discrepancies are greatest over the desert, where a positive precipitation change may lead to a slightly negative runoff change due to enhanced AET (e.g. MIROC-ESM-CHEM). Overall, any precipitation change appears to control the runoff change. Because the precipitation changes are modest, so are the runoff change signals. For CNRM-CM5, the model with the strongest moistening, the average runoff signal over non-urban land surfaces is 34 mm/yr. The average runoff signal over non-urban land surfaces for the driest model, GFDL-CM3, is -21 mm/yr. Both values are small compared to the standard deviation of runoff in the baseline period (103 mm/yr).

We now turn to changes in PET and AET. As expected from the relationship between temperature and saturation vapor pressure, each future simulation projects a domain-wide increase in PET for all non-urban land surfaces (not shown), with an ensemble-mean change of 186 mm/yr averaged over non-urban land areas. PET increases are highest above 1000m, where decreases in future snow cover and albedo during winter lead to increased absorption of downward radiation, providing more energy for PET. Annual mean AET changes are shown in Fig. 5 (third row). Despite domain-wide PET increases, AET rates are severely limited by surface water availability. In fact, for the 5 dynamically downscaled GCMs, the sign of model's precipitation change is the main determinant of the model's AET change. The partitioning of the precipitation change into a runoff change or AET change is largely determined by baseline partitioning of precipitation into runoff and AET (Fig. 2.). However, the relationship between the precipitation change and AET change is not as strong as the relationship between the precipitation change and runoff change (model-average spatial correlation coefficient of $r = 0.61$ vs. $r = 0.88$).

c) Idealized simulations: Limited influence of warming on AET

It is noteworthy that the annual mean change in AET for each of the five dynamically-downscaled GCMs is small and precipitation-determined, even though there is significant near-surface warming. One would expect warmer surface air temperatures and increased downward longwave radiation to enhance AET throughout the domain at least somewhat. We turn to the idealized simulations to quantify the sensitivity of runoff and AET to warming in the absence of a precipitation change. By looking at differences between the idealized simulations and the baseline (1981-2000) simulation, we examine the direct influence of changing temperatures on annual mean AET and runoff.

Fig. 7. shows the change in annual 2-meter air temperature (first row) and annual AET (second row) for each of the idealized simulations: T2, T4 and T6. Due to a nearly negligible change in infiltration, the surface water balance equation constrains the runoff change for each simulation to be almost identical in magnitude to the AET change, with an opposite sign. For even the most extreme warming case (T6), the domain-average AET change over non-urban land surfaces (5.01 mm/yr) pales in comparison to both the baseline mean (232 mm/yr) and interannual variability (56 mm/yr). Runoff changes are similarly miniscule. The absolute change in domain-average evaporative fraction of precipitation (E/P) increases by 0.6% from the baseline simulation to T6 scenario, a tiny amount. The AET changes (second row) appear to have some spatial structure, in that the strongest AET increases are at high elevations (see topography in Fig. 1b) as well as at locations with high AET in the baseline (Fig. 2c). However, even for a mountain location where the AET signal is stronger (like the location referenced in Fig. 3a), annual AET in the T6

scenario increases by 11 mm/yr, a mere 2% relative increase. Without a precipitation change, surface air temperatures would have to increase significantly more than 6º C to have a substantial impact on annual AET and runoff.

The insensitivity of surface hydrology to warming is explored further in Fig. 8, which shows the average annual cycles of PET and AET over non-urban land surfaces for the baseline (1981-2000) simulation (blue), T2 (yellow), T4 (red) and T6 (black). In Fig. 8a, PET increases significantly in all idealized simulations following the monthly temperature distribution. Domain-average annual PET increases by 5%, 10% and 15% for T2, T4 and T6, respectively.

In contrast, AET (Fig. 8b) remains largely unchanged in all three idealized cases. This is an artifact of Southern California's Mediterranean climate (discussed in section 1), in which the annual cycles of precipitation and soil moisture are out of phase with that of PET. In the case of T2, T4 and T6, PET increases are strongest during the months of April to October (Fig. 8a), yet soil moisture is relatively low from July to January (in both the baseline and idealized simulations) due to the seasonality of precipitation. As a result, only the months of April through June in the idealized scenarios have both significantly enhanced PET and relatively moist soils. For the most extreme warming scenario (T6), this overlap of enhanced PET and soil moisture availability leads to monthly AET increases of 7.8%, 6.5% and 5% for April, May and June, respectively (Fig. 8b). The April to June AET change then accelerates the soil moisture decrease that occurs in the baseline simulation from May to July. This exhausts nearly the same amount of soil moisture as in the baseline, but earlier in the season, with little effect on annual mean runoff. The remaining months of July through March have either limited soil moisture or relatively low

PET, prohibiting increases in annual total AET. Thus annual mean runoff and AET are largely insensitive to warming. One could imagine a very different situation if the study domain received significant summer rainfall, which would cause elevated soil moisture values at the same time as the peak in the annual PET cycle. In this case, warming could lead to enhanced AET and decreased annual mean runoff.

This insensitivity of annual mean runoff and AET to future temperature changes in Southern California is consistent with other studies over Northern California. Risbey and Entekhabi (1996) found annual mean streamflow in the Sacramento River to be nearly insensitive to temperature changes, but very sensitive to precipitation changes. Dettinger et al. (2004) found similar results in the Merced, Carson and American river basins of California. Together, the dynamically-downscaled GCMs and idealized simulations suggest both annual mean runoff and AET in the Los Angeles region are almost insensitive to warming, but highly sensitive to changes in annual mean precipitation.

5. Summary and conclusions

Although it has been well documented that climate change is likely to have profound impacts on the hydrology of the Western United States, few studies have examined the sensitivity of surface hydrology in the Los Angeles region to climate change. Without such analysis, the scientific foundation for informed adaptation strategies at the local and regional scale is missing. This study aims to close this knowledge gap by exploring sensitivities of both annual runoff and AET to regional precipitation and temperature changes.

This study uses dynamical-downscaling techniques to examine mid-21st century changes to surface hydrology over the Los Angeles region under RCP8.5 for five CMIP5 GCMs: CCSM4, CNRM-CM5, GFDL-CM3, MIROC-ESM-CHEM and MPI-ESM-LR. Any change in annual precipitation is mirrored by a similar, though weaker, change in runoff. However, the average annual precipitation change over non-urban land surfaces for each GCM is small compared to their range of baseline interannual variability. Despite the warming projected by the dynamically-downscaled GCMs in this study, annual mean runoff and AET signals are also found to be well within their range of baseline interannual variability.

Given the small precipitation change, this study includes a series temperature sensitivity experiments to shed light on the hydrologic insensitivity to warming. Three idealized simulations are performed in which the baseline climate is perturbed by uniform near-surface air temperature increases of 2º, 4º and 6º C. Significant increases in annual mean PET occur with increasing temperatures, with strongest increases in the warm months. Despite significantly enhanced April to October PET in the idealized warming scenarios, available soil moisture confines AET increases to the months of April through June. Small springtime AET increases accelerate soil moisture drying, but exhaust nearly the same amount of moisture, leading to miniscule changes in annual mean runoff and AET for all idealized scenarios. This is an artifact of the out-of-phase relationship between the annual precipitation and soil moisture cycles and annual PET cycle in Mediterranean-type climate zones like the Los Angeles region.

The finding that annual mean runoff is nearly insensitive to temperature increases in the Los Angeles region may have implications for other Mediterranean climate regions. Surface hydrology in other Mediterranean climate zones, including most lands around the Mediterranean Sea, Western and Southern Australia, and Chile, is similar to that of the Los Angeles region, and would likely respond in a similar manner to warming. Previous studies of warming impacts to surface hydrology in Mediterranean-type climates outside California have indeed shown similar results. Chiew et al. (1995) applied a range of plausible temperature and precipitation changes to a rainfall-runoff model to study the sensitivity of runoff and soil moisture in Australian catchments to potential changes in climate. They found that compared to precipitation, temperature increases alone have negligible impacts on runoff and soil moisture. New (2002) examined the sensitivity of runoff in four mountainous catchments in the southwestern Cape of South Africa to a range of possible future climate changes, and found that streamflow in all catchments is more responsive to precipitation changes than PET changes.

One potential limitation of this study is that the modeling framework does not take into consideration the physiological effects of increased atmospheric carbon dioxide concentrations on plant stomatal resistance (i.e. CO_2 fertilization). Increases in atmospheric carbon dioxide concentrations enhance the leaf's internal carbon dioxide absorption rate. This gives plants the flexibility to increase their stomatal resistance to conserve water. CO_2 fertilization generally results in a decrease of canopy transpiration and therefore affects the water balance (Betts et al. 2007). In our simulations, the CO_2 fertilization effect would reduce AET sensitivity to temperature increases still further by reducing AET. Therefore, if this study had included CO_2

fertilization effects, the result that annual mean AET and runoff are nearly insensitive to temperature increases would hardly change.

This study diagnoses the sensitivity of the Los Angeles region's surface hydrology to both precipitation and temperature changes. Together, the dynamically-downscaled GCMs and idealized simulations suggest both annual mean runoff and actual evapotranspiration in the Los Angeles region are almost insensitive to warming, but are instead controlled by possible changes in annual mean precipitation. Surface hydrology in other Mediterranean climate regions will likely behave similarly. This result greatly mitigates a potential vulnerability of water resources to a changing climate in an important semi-arid region of the world. It also reveals that a regional climate change adaptation strategy relying on local water resources is a viable one.

Acknowledgments

Support for this work was provided by the City of Los Angeles and the US Department of Energy as part of the American Recovery and Reinvestment Act of 2009. Additional funding was provided by the National Science Foundation (Grant #EF-1065863, "Collaborative Research: Do Microenvironments Govern Macroecology?").

References

Adam, J.C., A.F. Hamlet, D.P. Lettenmaier, 2009: Implications of global climate change for snowmelt hydrology in the twenty-first century. Hydrol. Process. 23, 962–972.

Baldocchi, D., et al., 2001: FLUXNET: A new tool to study the temporal and spatial variability of ecosystem-scale carbon dioxide, water vapor, and energy flux densities. Bull. Am. Meteorol. Soc., 82(11), 2415–2434.

Barnett, T.P., D.W. Pierce, H.G. Hidalgo, C.B. Benjamin, D. Santer, T. Das, G. Bala, A.W. Wood, T. Nozawa, A.A. Mirin, D.R. Cayan, and M.D. Dettinger, 2008: Human-induced changes in the hydrology of the Western United States. Science, 319, 1080–1083.

Barrera-Escoda, A., M. Gonçalves, D. Guerreiro, J. Cunillera, J.M. Baldasano, 2013: Projections of temperature and precipitation extremes in the North Western Mediterranean Basin by dynamical downscaling of climate scenarios at high resolution (1971–2050). Climatic Change pp 1–16. doi:10.1007/s10584-013-1027-6.

Bates, B.C., Z.W. Kundzewics, S. Wu, and J.P. Palutikof, 2008: Climate Change and Water. Technical Paper of the Intergovernmental Panel on Climate Change. IPCC Secretariat, Geneva, Switzerland, 210 pp.

Berg, N., A. Hall, F. Sun, S. Capps, D. Walton, B. Langenbrunner, and J. Neelin, 2015: Twenty-First-Century Precipitation Changes over the Los Angeles Region. J. Climate, 28, 401-421. doi:10.1175/JCLI-D-14-00316.1

Betts, R.A., O. Boucher, M. Collins, P.M Cox, P.D. Falloon, N. Gedney, D.L. Hemming, C. Huntingford, C.D. Jones, D.M.H. Sexton, and M. Webb, 2007: Projected increase in continental runoff due to plant responses to increasing carbon dioxide. Nature, 448, 1037-1042.

Blanco, H. P., J. Newell, L. Stott, M. Alberti, 2012: Water Supply Scarcity in Southern California: Assessing Water District Level Strategies. Los Angeles, CA: Center for Sustainable Cities, Price School of Public Policy, University of Southern California. http://sustainablecities.usc.edu/research/Chapter%203.%20LADWP%2012%2019%20p.pdf

Caldwell, P., H.N.S. Chin, D.C. Bader, and G. Bala, 2009: Evaluation of a WRF dynamical downscaling simulation over California. Climatic Change, 95, 499-521.

Cayan, D.R., 1996: Interannual climate variability and snowpack in the western United States. Journal of Climate, 9, 928-948.

Chiew, F.H.S., P.H. Whetton, T.A. McMahon, and A.B. Pittock, 1995: Simulation of the impacts of climate change on runoff and soil moisture in Australian catchments. Journal of Hydrolgy, 167, 121‐147.

Chen, F., and J. Dudhia, 2001: Coupling an advanced land surface-hydrology model with the

Penn State-NCAR MM5 modeling system. Part I: Model implientation and sensitivity. Mon. Wea. Rev., 129, 569-585. doi:10.1175/1520-0493(2001)129,0569: CAALSH.2.0.CO;2.

City of Camarillo, 2010: *Urban Water Management Plan 2010*. Available at http://www.water.ca.gov/urbanwatermanagement/2010uwmps/Camarillo,%20City%20of/2010%20UWMP%20Final%20Draft.pdf

Conil, S. and A. Hall, 2006: Local regimes of atmospheric variability: A case study of Southern California. Journal of Climate, 19, 4308-4325.

Cowling R.M., P.W. Rundel, B.B. Lamont, M.K. Arroyo, M. Arianoutsou, 1996: Plant diversity in Mediterranean-climate regions. Trends in Ecology and Evolution, 11: 362–366

Cowling, R. M., F. Ojeda, B. B. Lamont, P. W. Rundel, and R. Lechmere-Oertel, 2005: Rainfall reliability a neglected factor in explaining convergence and divergence of plant traits in fire-prone mediterranean-climate ecosystems. Glob. Ecol. Biogeogr. 14: 509–519.

Dettinger, M.D., D.R. Cayan, M.K. Meyer, A.E. Jeton, 2004: Simulated hydrologic responses to climate variations and changes in the Merced, Carson, and American river basins, Sierra Nevada, California, 1900–2099. Clim. Change, 62, 283–317.

Ek, M. B., K. E. Mitchell, Y. Lin, E. Rogers, P. Grunmann, V. Koren, G. Gayno, J.D. Tarpley, 2003: Implementation of Noah land surface model advances in the National Centers for Environmental Prediction operational mesoscale Eta model. Journal of Geophysical Research, 108 (D22), 8851.

Flaounas, E., P. Drobinski, M. Vrac, S. Bastin, C. LebeaupinBrossier, M. Stefanon, M. Borga, and J. Calvet, 2012: Precipitation and temperature space–time variability and extremes in the Mediterranean region: Evaluation of dynamical and statistical downscaling methods. Climate Dynamics, 40: 2687–2705. DOI: 10.1007/s00382-012-1558-y.

Giorgi, F., and L. O. Mearns, 1991: Approaches to regional climate change simulation: A review. Rev. Geophys., 29, 191–216.

Hamlet, A., P. Mote, M. Clark, and D. Lettenmaier, 2005: Effects of temperature and precipitation variability on snowpack trends in the western United States. J. Climate, 18, 4545–4560.

Hara, M., T. Yoshikane, H. Kawase, and F. Kimura, 2008: Estimation of the impact of global warming on snow depth in Japan by the pseudo-global warming method. Hydrol. Res. Lett., 2, 61–64.

Huang, G., Kadir, T. and F. Chung, 2012: Hydrological response to climate warming: The Upper Feather River Watershed, Journal of Hydrology, Volumes 426–427, 138-150.

Hughes M., A. Hall, R.G. Fovell, 2007: Dynamical controls on the diurnal cycle of temperature in complex topography. Climate Dynamics, 29, 277-292.

IPCC [Intergovernmental Panel on Climate Change]. 2014. Climate Change 2014: Impacts, adaptation and vulnerability. Part A: Global and Sectoral Aspects. Contribution of Working Group II to the Fifth Assessment Report of the Intergovernment Panel on Climate Change. Field C. B., V.R. Barros, D.J. Dokken, K.J. Mach, M.D. Mastrandrea, T.E. Bilir, M. Chatterjee, K.L. Ebi, Y.O. Estrada, R.C. Genova, B. Girma, E.S. Kissel, A.N. Levy, S. MacCracken, P.R. Mastrandrea, and L.L. White (eds.) Cambridge University Press, Cambridge, United Kingdom and New York, NY, USA, 1132 pp.

Kanamitsu, M., and H. Kanamaru, 2007: Fifty-seven-year California reanalysis downscaling at 10 km (CaRD10). Part I: system detail and validation with observations. Journal of Climate, 20 (22), 5553–5571.

Kapnick, S., and A. Hall, 2010: Observed climate-snowpack relationships in California and their implications for the future. J. Clim. 23: 3446-3456, DOI:10.1175/2010JCLI203.1

Kawase, H., T. Yoshikane, M. Hara, F. Kimura, T. Yasunari, B. Ailikun, H. Ueda, and T. Inoue, 2009: Intermodel variability of future changes in the Baiu rainband estimated by the pseudo global warming downscaling method. J. Geophys. Res., 114, D24110, doi:10.1029/2009JD011803.

Kottek, M., Grieser, J., Beck, C., Rudolf, B., Rubel, F., 2006. World Map of the Köppen–Geiger climate classification updated. Meteorol. Z. 15, 259–263. doi:10.1127/ 0941-2948/2006/0130.

Leung, L.R., Y. Qian, X. Bian, 2003: Hydroclimate of the western United States based on observations and regional climate simulations of 1981-2000. Part I: seasonal statistics. Journal of Climate, 16, 1892-1911.

Leung L.R., Y. Qian, X. Bian, W.M. Washington, J. Han, J. Roads, 2004: Mid-century ensemble regional climate change scenarios for the western United States. Climatic Change 62, 75– 113.

Lins, H.F, 2012: USGS Hydro-Climatic Data Network 2009 (HCDN-2009). U.S. Geological Survey Fact Sheet. 2012-3047. http://pubs.usgs.gov/fs/2012/3047.

Long Beach Water Department, 2010: *Urban Water Management Plan.* Available at http://www.water.ca.gov/urbanwatermanagement/2010uwmps/Long%20Beach%20Water%20Department/2010%20UWMP%20-%20Revised%20110915%20-%20FINAL.pdf

Masiokas, M., R. Villalba, B. Luckman, C. Le Quesne and J.C. Aravena, 2006: Snowpack variations in the Central Andes of Argentina and Chile, 1951–2005. Large-scale atmospheric influences and implications for water resources in the region. J. Climate 19, 6334–6352.

Maurer, E.P, 2007: Uncertainty in hydrologic impacts of climate change in the Sierra Nevada, California under two emissions scenarios Clim. Change, 82 (3–4), 309–325.

Mesinger, F., G. DiMego, E. Kalnay, K. Mitchell, P.C. Shafran, W. Ebisuzaki, and W. Shi, 2006: North American regional reanalysis. Bull. Amer. Meteor. Soc., 87(3), 343–360.

Myers, N., R. A. Mittermeier, C. G. Mittermeier, G. A. B. da Fonseca, and J. Kent, 2000: Biodiversity hot spots for conservation priorities. Nature 403:853–858.

New, M., 2002: Climate change and water resources in the southwestern Cape, South Africa. South African Journal of Science, 98: 369–376.

Pan, L.-L., S.-H. Chen, D. Cayan, M.-Y. Lin, Q. Hart, M.-H. Zhang, Y. Liu, J. Wang, 2011: Influences of climate change on California and Nevada regions revealed by a high- resolution dynamical downscaling study. Climate Dynamics, 37, 2005-2020.

Paton, F. L., H. R. Maier, and G. C. Dandy, 2013): Relative magnitudes of sources of uncertainty in assessing climate change impacts on water supply security for the southern Adelaide water supply system, Water Resour. Res., 49, 1643–1667, doi:10.1002/wrcr.20153.

Pierce, D.W., T. Das, D.R. Cayan, E.P. Maurer, N.L. Miller, Y. Bao, M. Kanamitsu, K. Yoshimura, M.A. Snyder, L.C. Sloan, G. Franco, and M. Tyree, 2012: Probabilistic estimates of future changes in California temperature and precipitation using statistical and dynamical downscaling. Clim. Dyn.,

Qian, Y., S.J. Ghan, L.R. Leung, 2009: Downscaling hydroclimatic changes over the Western U.S. Based on CAM subgrid scheme and WRF regional climate simulations, International Journal of Climatology, 30, 675-693.

Rasmussen, R. and Coauthors, 2011: High-Resolution Coupled Climate Runoff Simulations of Seasonal Snowfall over Colorado: A Process Study of Current and Warmer Climate. J. Climate, 24, 3015–3048

Ratnam, J.V., S. K. Behera, S. B. Ratna, C. J. de W. Rautenbach, C. Lennard, J.-J. Luo, Y. Masumoto, K. Takahashi, and T. Yamagata, 2013: Dynamical Downscaling of Austral Summer Climate Forecasts over Southern Africa Using a Regional Coupled Model. J. Climate, 26, 6015–6032. doi: http://dx.doi.org/10.1175/JCLI-D-12-00645.1

Risbey, J.S. and D. Entekhabi, 1996: Observed Sacramento Basin streamflow response to precipitation and temperature changes and its relevance to climate impact studies J. Hydrol., 184, 209–223.

Roos, M., 1991. A trend of decreasing snowmelt runoff in northern California. In: 59th Western Snow Conference, Juneau, AK, pp. 29–36.

Schär, C., C. Frei, D. Lüthi, and H. C. Davies, 1996: Surrogate climate-change scenarios for regional climate models. Geophys. Res. Lett., 23(6), 669–672. doi:10.1029/96GL00265.

Skamarock, W.C., Klemp J.B., Dudhia J., Gill D.O., Barker D.M., Duda M.G., Huang X-Y, Wang W., Powers J.G., 2008: A Description of the Advanced Research WRF Version 3. NCAR Technical Note, NCAR/TN-475+STR.

Slack, J. R., A. M. Lumb, and J. M. Landwehr, 1993: Hydroclimatic data network (HCDN): A U.S. Geological Survey streamflow data set for the United States for the study of climate variation, 1874–1988, U.S. Geol. Surv. Water Resour. Invest. Rep. [CD-ROM], 93-4076.

Sun F., D Walton, and A Hall, 2015a: A hybrid dynamical–statistical downscaling technique, part II: End-of-century warming projections predict a new climate state in the Los Angeles region. Journal of Climate, in press.

Sun F., A. Hall, M. Schwartz, D. Walton and N. Berg, 2015b: 21st-century snowfall and snowpack changes over the southern California mountainous region. Journal of Climate, submitted.

Taylor, K. E., R. J. Stouffer, and G. A. Meehl, 2012: An overview of CMIP5 and the experiment design. Bull. Amer. Meteor. Soc., 93(4), 485–498.

Vicuna, S., E.P. Maurer, B. Joyce, J.A. Dracup, D. Purkey, 2007: The Sensitivity of California water resources to climate change scenarios J. Am. Water Resour. Assoc., 43, 482–498

Walton D., F. Sun, A. Hall and S. Capps, 2015: A Hybrid Dynamical-Statistical Downscaling Technique, Part I: Development and Validation of the Technique. Journal of Climate, in press.

Young, C.A., M. Escobar, M. Fernandes, B. Joyce, M. Kiparsky, et al., 2009: Modeling the Hydrology of California's Sierra Nevada for Sub-Watershed Scale Adaptation to Climate Change. J. Am. Water Resour. Assoc. (JAWRA), 45 (6), 1409-1423.

Ziervogel, G., P. Johnston, M. Matthew and P. Mukheibir, 2010: Using climate information for supporting climate change adaptation in water resource management in South Africa. Climatic Change,103: 537–554. DOI 10.1007/s10584-009-9771-3.

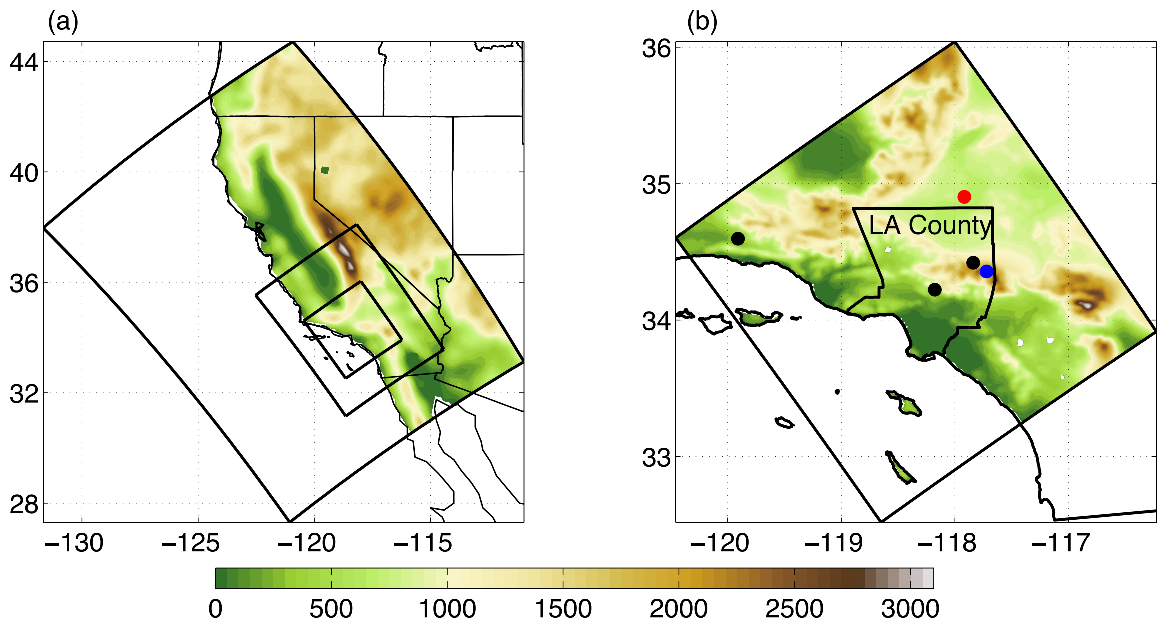

FIG. 1: a) Model setup, with three nested WRF domains at resolutions of 18, 6, and 2 km. Topography (m) is shown at the resolution of the 18km domain in color and black lines show boundaries for US states. (b) Topography of the innermost domain (2- km resolution) of the regional simulation, with the border of Los Angeles County in black. In (b), black circles indicate locations of the 3 gauges used for streamflow validation. The blue and red circles in (b) indicate the mountain location and desert location, respectively, referenced in Fig. 3 and section 2b.

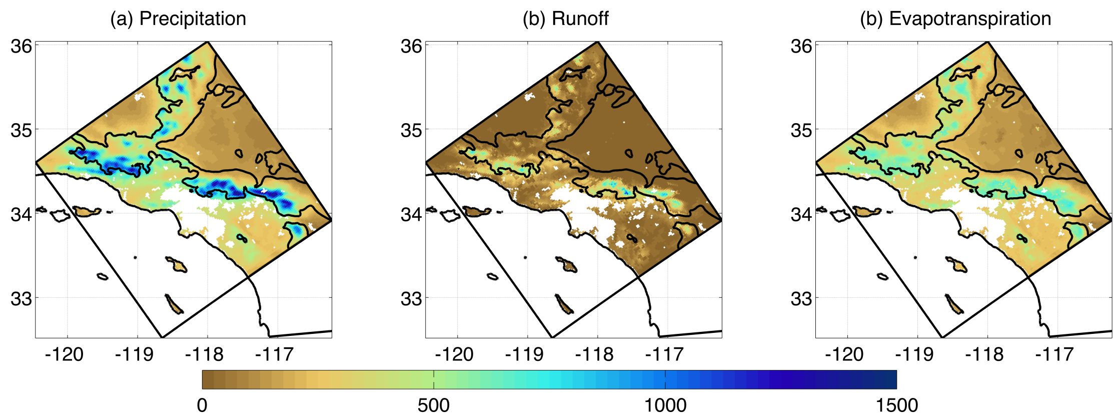

FIG. 2: Noah-LSM/WRF simulation of annual a) accumulated precipitation, b) runoff and c) actual evapotranspiration for the baseline (1981-2000) period. Unit is mm/yr. The 1000m topography contour is highlighted in black. Grid cells with missing values are urban or over water surfaces.

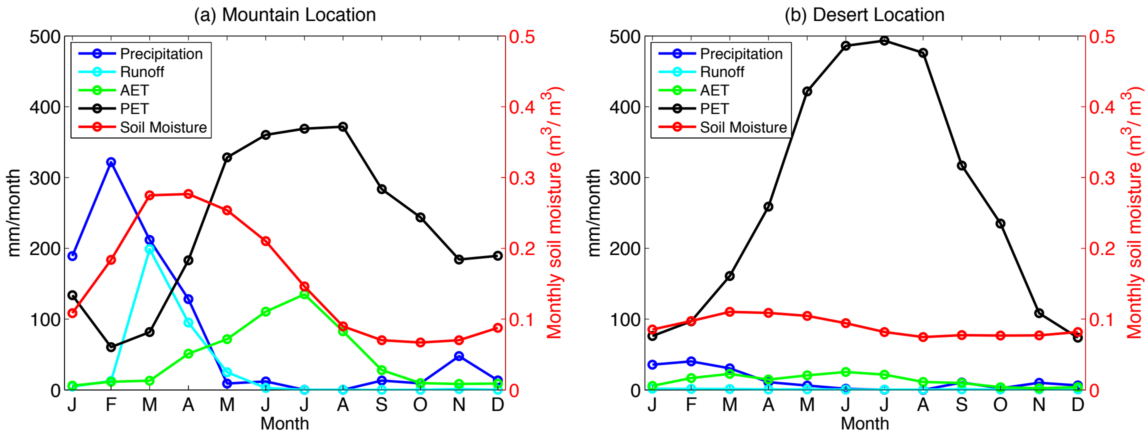

FIG. 3: Noah-LSM/WRF simulation of the mean annual cycle of the water balance at a point representative of (a) mountain locations and (b) the inland desert. Monthly accumulated values (unit: mm/month) of precipitation (blue), runoff (cyan), actual evapotranspiration (green) and potential evapotranspiration (black) are shown with respect to the left y-axis. The climatological monthly soil moisture (unit: m^3/m^3) of the top 2m of the soil column is also shown (red) with respect to the right y-axis.

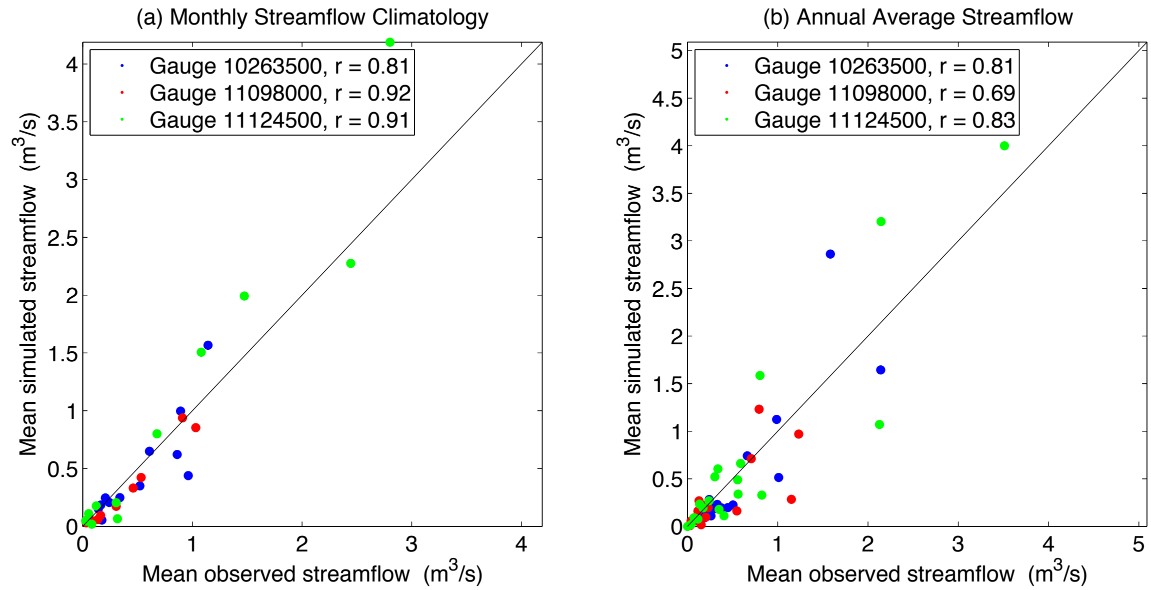

FIG. 4: Evaluation of Noah-LSM/WRF dynamical downscaling of runoff during the baseline period for three streamflow gauges. a) Observed vs. simulated monthly mean streamflow. b) Observed vs. simulated annual mean streamflow. Observed streamflow data is compared to simulated surface runoff aggregated upstream of the gauge within a watershed. Correlation coefficients for each gauge are also presented. The line y = x is shown in black.

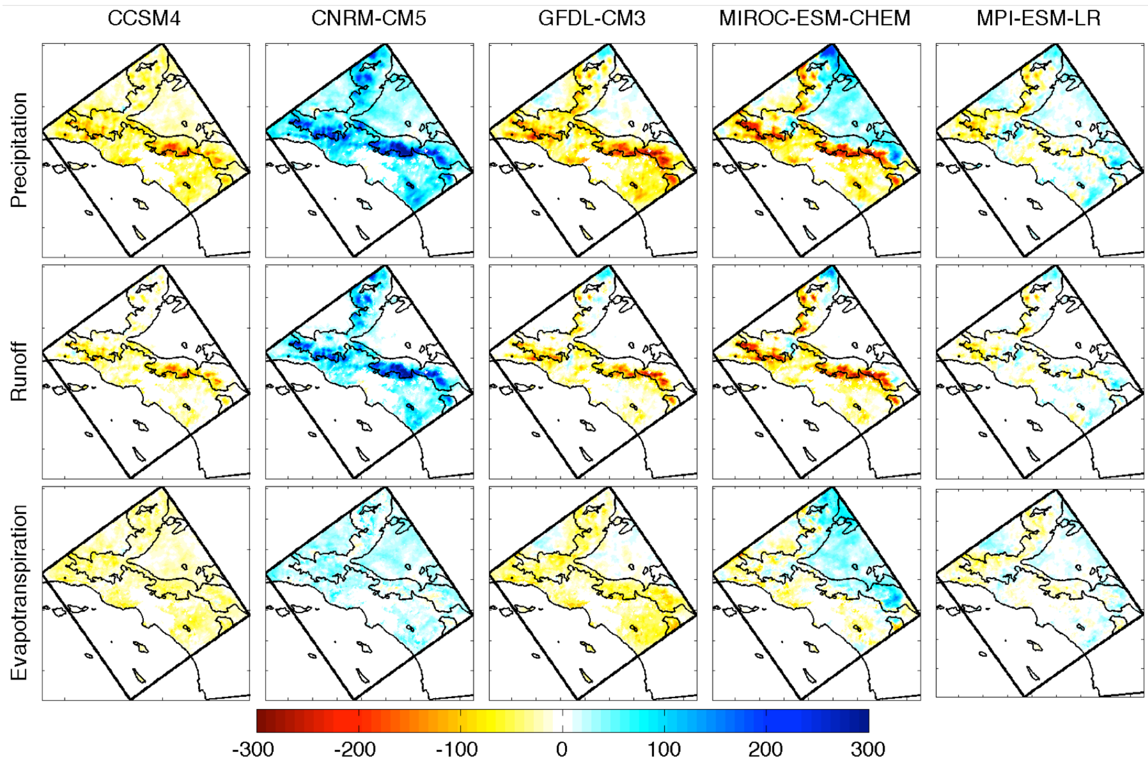

FIG. 5: Noah-LSM/WRF simulation of the mid-21st century change (mm/yr) in precipitation (row 1), runoff (row 2) and actual evapotranspiration (row 3) relative to the baseline period for five GCMs under RCP8.5: CCSM4, CNRM-CM3, GFDL-CM3, MIROC-ESM-CHEM and MPI-ESM-LR. Blue shading indicates moistening, while yellow/red shading indicates drying. The 1000m topography contour is highlighted.

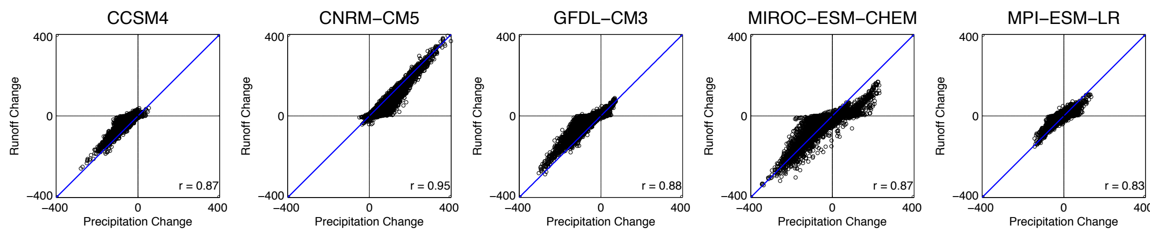

FIG. 6: Scatter plot of mid-21st century change in annual precipitation (mm/yr) vs. annual runoff (mm/yr) at all non-urban land surface in the study domain when five GCMs under RCP8.5 are downscaled: CCSM4, CNRM-CM3, GFDL-CM3, MIROC-ESM-CHEM and MPI-ESM-LR. Correlation coefficients are shown in the bottom corner for each plot. The line y = x is shown in blue.

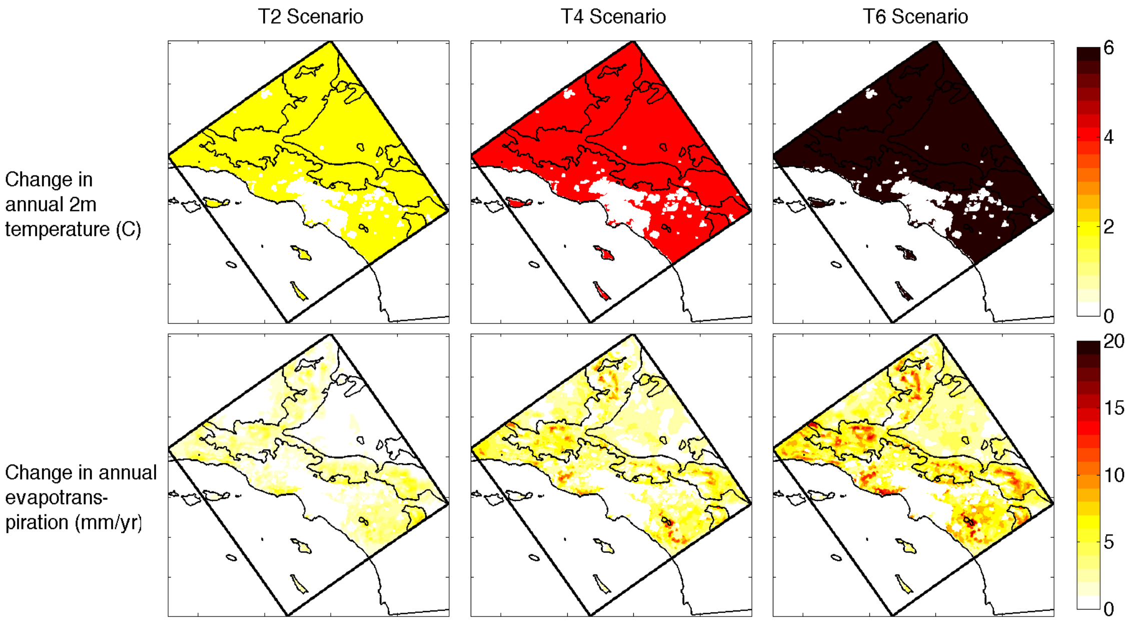

829
830 FIG. 7: Results from three idealized simulations in which Noah-LSM/WRF dynamically-
831 downscaled output for the baseline (1981-2000) period is perturbed by a uniform increase in
832 near-surface air temperature of 2° C (left column, T2 scenario), 4° C (center column, T4
833 scenario), and 6° C (right column, T6 scenario). Changes in annual near-surface air temperature
834 (first row, unit: °C) and actual evapotranspiration (second row, unit: mm/yr) are shown for each
835 idealized scenario. Precipitation is not perturbed. The 1000m topography contour is shown.
836

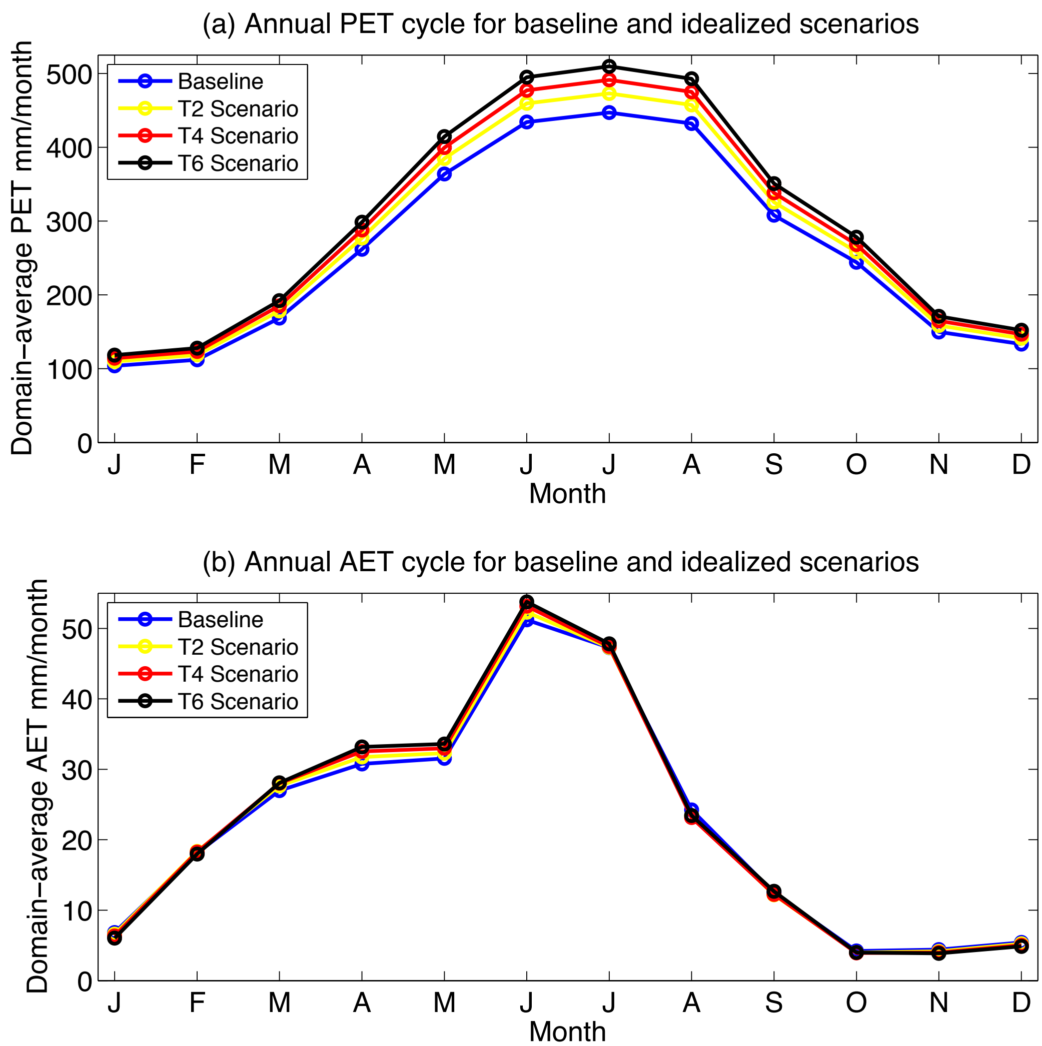

FIG. 8: Noah-LSM simulation of the domain-average annual cycle of (a) potential evapotranspiration and (b) actual evapotranspiration over non-urban land surfaces for the baseline (1981-2000) simulation (blue) and three idealized simulations in which the baseline simulation is perturbed by a uniform increase in near-surface air temperature of 2° C (yellow, T2 scenario), 4° C (red, T4 scenario), and 6° C (black, T6 scenario). Unit: mm/month.